Hindawi
Advances in Materials Science and Engineering
Volume 2022, Article ID 1968770, 17 pages
https://doi.org/10.1155/2022/1968770

*Research Article*

# Durability of Marine Concretes with Nanoparticles under Combined Action of Bending Load and Salt Spray Erosion

**Zhang Maohua, Lv Zhengyi, Cui Jiyin, Tian Zenong, and Li Zhiyi**

*School of Civil Engineering, Northeast Forestry University, Harbin 150040, China*

Correspondence should be addressed to Zhang Maohua; zmh7716@163.com

Received 15 March 2022; Accepted 3 July 2022; Published 2 August 2022

Academic Editor: Mehmet Emiroğlu



The coupling effect of bending load and salt spray erosion during the service of a sea-crossing bridge accelerates the deterioration and durability of concrete and dramatically reduces the load-carrying capacity of the bridge. The effects of nanoparticles on the durability of marine concrete exposed to bending loads and salt spray erosion were studied. In this paper, nano-$SiO_2$ and nano-$Fe_2O_3$ were mixed into plain concrete. Free chloride ions ($Cl^-$) were titrated at different concrete depths using a four-point loading device and a self-developed salt spray erosion test chamber. Test results showed that chloride ion levels in the tensile and compressive zones for both nanoconcretes were lower than plain concrete at the same timepoint. The optimal mixtures of the two nanoparticles were 2% and 1%, and the improvement of nano-$SiO_2$ was more significant than nano-$Fe_2O_3$. Due to the special properties of nanomaterials, they effectively improved the microstructure of concrete and the composition of cement hydration products. This allowed concrete to become more compact, reduced crack generation, increased the difficulty of $Cl^-$ migration inside the concrete, and improved the overall durability of marine concrete upon exposure to bending loads and salt spray erosion.

## 1. Introduction

With the recent and rapid development of the Chinese national economy, cross-sea bridges in China have also ushered in a new era. For bridges in long-term marine environments, not only the upper structures are located in the salt spray zone, and $Cl^-$ in the salt spray will significantly influence the service life of a sea-crossing bridge, [1–3] but also subject to long-term bending load. Over time, the coupling effect of bending load and salt spray erosion corrodes the steel reinforcement in the bridge structure, which results in a durability loss and has become an important problem affecting the service life of marine concrete structures. Therefore, the durability study of marine concrete under the coupling effect of bending load and salt spray erosion is of great importance to engineering practice.

In recent years, a lot of experimental work has been done by domestic and foreign scholars to study the durability of marine concrete under the coupled attack of chloride and external load; the forms of loading include fatigue loading, bending loading, compressive loading, and tensile loading. Under the chloride ion environment, several studies [4–6] applied fatigue loading to reinforce concrete beams, and the flexural performance and fatigue life of reinforced concrete beams were discussed. As the number of fatigue loads increases, chloride ions accelerate the corrosion of concrete beams, resulting in a significant reduction in fatigue life. Wu et al. [7, 8] concluded that the reinforcement rate also changes the rate of chloride ion attack, considering the effects of different fatigue load levels and reinforcement rates, and propose a model for the service life of reinforced concrete beams. Compared with fatigue loads (cyclic loads), other external loads such as bending loads (static loads), compressive loads, and tensile loads, when they are coupled with chloride ion attack, they also cause gradual deterioration of the concrete [9–13] and microcracks in the internal structure and cracks on the surface [14–16], ultimately leading to a significant reduction in the service life of the concrete structure.

With the improvement of the scientific and technological level, many scholars have studied the improvement of durability of concrete loaded in chloride attack environment

Table 1: Performance of nanoparticles.

| Item | Diameter (nm) | Surface properties | Purity (%) | Specific surface area ($m^2/g$) | Phase | pH |
|---|---|---|---|---|---|---|
| $SiO_2$ | 25 | Hydrophilic | 99.5 | 190–250 | — | 5–7 |
| $Fe_2O_3$ | 90 | Hydrophilic | 99.7 | 60 | $\alpha$ | — |

by adding appropriate admixtures [13], fiber compounds [1, 17], and coral aggregates [18]. Few studies have been reported on the durability performance of nanoconcrete under both bending load and salt spray erosion. Due to their small size, nanomaterials possess many properties that conventional materials do not possess. The addition of nanomaterials to normal concrete has essential effects on the hydration of cement and the microstructure of concrete that include reducing porosity and improving C-S-H gel properties [19, 20]. Therefore, adding nanomaterials to normal concrete improves the durability performance of concrete as well as the bending load and salt spray erosion.

In this paper, nano-$SiO_2$ and nano-$Fe_2O_3$ were selected to replace cement in equal amounts and incorporated into marine concrete. A modified four-point bending loading equipment and a concrete durability test chamber under the action of salt spray erosion was developed independently. They were used to conduct the durability test on ordinary concrete and nanoconcretes under the coupling action of bending load and erosion by salt spray. The study was carried out from four aspects of nanoparticles admixture, depth, age, and stress ratio; and the pattern of free $Cl^-$ content in concrete and nanoconcrete was analyzed; and finally, the strengthening mechanism of nano-$SiO_2$ and nano-$Fe_2O_3$ reinforced concrete is discussed. This work will provide a durability design solution for marine engineering structures.

## 2. Test Materials and Methods

### 2.1. Test Materials

(1) Cement: P.O42.5 ordinary silicate cement produced by Harbin Cement Plant

(2) Fine aggregate: river sand with a fineness modulus of 2.42, medium sand

(3) Coarse aggregate: the choice of particle size 5–31.5 mm continuous gravel gradation

(4) Defoamer agent: tributyl phosphate was selected as the defoamer to reduce air bubbles generated when the nanomaterials were mixed into the concrete

(5) Water reducing agent: a high-efficiency water-reducing agent with NDF-type naphthalene was used, and its amount was determined according to the method specified in the concrete admixture (GB8076-2008)

(6) Salt solution: to simulate the natural marine environment and ensure test progress, a 5% NaCl solution was utilized

(7) Nano-materials: nano-$SiO_2$ and nano-$Fe_2O_3$ produced by Hangzhou Hengge Nanotechnology Co. Nanoparticle properties are shown in Table 1

### 2.2. Concrete Ratio.

According to the code for durability design of concrete structures (GB/T50476-2019) and the proportional design procedure for plain concrete (JGJ55-2011), the environmental action level is III-c under the marine chloride environment. Combined with the slump requirement, the concrete design strength level was C45, the water-cement ratio was 0.44, the sand rate was 33%, the water-reducing agent level was 0.25% of the cement dosage, and the amount of defoamer was 4% of the water reducing agent dosage. Nanoconcrete is based on a normal concrete ratio, maintaining the water-cement ratio and unit water consumption, but replacing cement with nanomaterials of equal quality and using four different amounts of nanomaterials (0.5%, 1.0%, 2.0%, and 3.0%). The concrete proportions are shown in Table 2.

### 2.3. Test Program

*2.3.1. Compressive and Flexural Strength Test of Concrete.* According to the Standard for Mechanical Properties Test Methods of General Concrete (GB/T50081-2019), concretes were cured for 28 d before compressive and flexural strength tests. Compressive strength tested each group of three $100 \times 100 \times 100$ mm specimens; flexural strength tested each group of three $100 \times 100 \times 400$ mm prismatic specimens:

(1) Number and size of test blocks: the tests used $100 \times 100 \times 400$ mm prismatic test blocks for a total of nine groups; each group contained 63 blocks, of which 60 were used for bending load and salt spray erosion coupling tests, and the remaining three blocks were only tested for salt spray erosion (see Figure 1).

(2) Test loading devices: the test reference [21] designed loading device and self-assembled a set of bending loading device (Figure 2); the advantages of the loading device is small size, easy to operate when loading and unloading, can intuitively control the size of the stress ratio, and can be placed directly in the salt spray test chamber. For protecting the loading device, a layer of antierosion paint was applied to the steel plate, roller, nut, and screw of the loading device, and a layer of machine oil was brushed on the threads and fillet of the upper part of the screw.

(3) Test loading method: a four-point bending loading method was employed. The stress ratio ($\sigma$) was controlled at 0.2, 0.3, 0.5, and 0.6 by tightening the uppermost bolt to load the specimen, and the stress level was controlled by the pressure transducer produced by the Anhui Bengbu Jinnuo Sensor Company. Because the test period length and stress relaxation may occur, the test process should be

Table 2: Mix proportion of concretes (unit: kg/m$^3$).

| Mixture type | Water | Cement | Sand | Coarse aggregate | FDN | Defoamer | Nanoparticles |
|---|---|---|---|---|---|---|---|
| PC | 205 | 486.0 | 638 | 1185 | 1.90 | — | — |
| NS05 | 205 | 483.6 | 638 | 1185 | 1.90 | 0.08 | 2.4 |
| NS10 | 205 | 481.1 | 638 | 1185 | 1.90 | 0.08 | 4.9 |
| NS20 | 205 | 476.3 | 638 | 1185 | 1.90 | 0.08 | 9.7 |
| NS30 | 205 | 471.4 | 638 | 1185 | 1.90 | 0.08 | 14.6 |
| NF05 | 205 | 483.6 | 638 | 1185 | 1.90 | 0.08 | 2.4 |
| NF10 | 205 | 481.1 | 638 | 1185 | 1.90 | 0.08 | 4.9 |
| NF20 | 205 | 476.3 | 638 | 1185 | 1.90 | 0.08 | 9.7 |
| NF30 | 205 | 471.4 | 638 | 1185 | 1.90 | 0.08 | 14.6 |

(a) (b)

Figure 1: (a) Compressive strength tests. (b) Flexural strength tests.

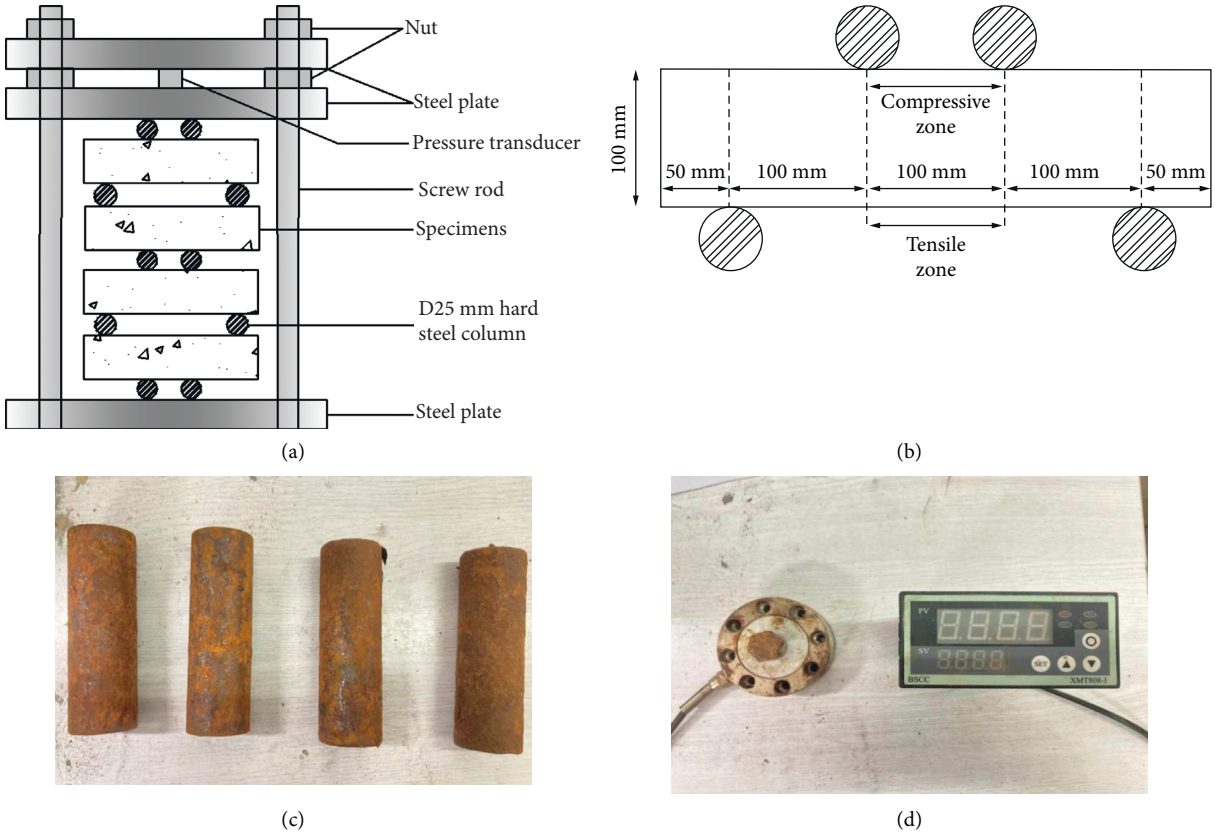


(a) (b)

(c) (d)

Figure 2: (a) Schematic diagram of the loading equipment. (b) 25 mm hard steel column arrangement and drilling positions in tensile and compressive zone diagram. (c) 25 mm hard steel column. (d) Pressure transducer.

periodically supplemented by the specimen load, which should be maintained.

(4) Salt spray erosion test: it refers to the neutral salt spray test (NSS test), a concrete durability test chamber under salt spray erosion (patent number ZL202120853835.7) (Figure 3).

In Figure 3, 1: thermocouple; 2: U-shaped bar; 3: wire; 4: spraying device; 5: temperature sensor; 6: inlet pipe; 7: drainage pipe; 8: water tank; 9: water pump; 10: nonreturn valve; 11: exhaust pipe; 12: exhaust fan; 13: sodium chloride solution. (a) is the mounting position of the U-shaped bar.

It consists of three systems as the main body, including (a) a thermostatic system consisting of three parts: thermocouple (1), temperature sensor (5), and U-shaped bar (2), fixed to the pp-board box. The thermostat (1), the temperature sensor (5), and the U-shaped bar (2) are connected by means of a wire (3). The spraying system (b) consists of three parts: spraying tray (4), water tank (8), and water pump (9), with an inlet pipe (6) and a drainage pipe (7) connected at the spraying tray (4), allowing the inlet pipe (6) to be connected to the water pump (9), and the drainage pipe (7) to be placed in the water tank (8). The exhaust system (c) consists of a nonreturn valve (10) and an exhaust fan (12) in two parts, with an exhaust pipe (11) connected to the exhaust fan (12) at side wall *d*. The test was conducted using continuous spraying (12 h continuous spraying with a 12 h break per day) (see Figure 4).

The test ages were set as follows: 4 d, 7 d, 14 d, 21 d, and 30 d according to the test ages recommended by the NSS test. The following are the specific test steps.

(i) The preloaded concrete test blocks together with the loading device were put into the salt spray chamber (2). (ii) Heating the U-shaped bar (a) with electricity and observing the thermocouple (1) so that it reaches a predetermined temperature (35°C), and then the U-shaped bar stops heating. (iii) Turn on the water pump (9) in the tank (8) so that the sodium chloride solution (13) slowly flows from the inlet pipes (6) and (7) into the spray tray (4) inside the tank for spraying. The size of the spray volume is controlled by adjusting the knob on the spray tray (4) to meet the specification. (iv) After reaching the corresponding test cycle, open the round hole on the nonreturn valve (10) and exhaust the moisture with the exhaust fan (12); take out the loading device and remove the concrete test block from the device to collect the test data and then repeat the above operation steps until the final test is completed.

### 2.4. Sampling and Determination of $Cl^-$

(1) Sampling of $Cl^-$: remove the concrete specimen after reaching each test age and drill the powder at the tensile and compressive zones (100 mm) of each specimen group with a table drill at various depths (0–3 mm, 3–5 mm, 5–10 mm, 10–15 mm, 15–20 mm, 20–25 mm, and 25–30 mm). At each depth, take three copies of (each copy 10 g) powder as a group, each specimen was drilled for a total of 14 groups of 42 samples, sieved (0.63 mm), and placed in an oven for 2 h. The samples were removed, cooled to room temperature, and used for free $Cl^-$ content test. Figure 5 shows the specific steps.

(2) Determination of $Cl^-$: the procedure for determining the free $Cl^-$ content is shown in Figure 6.

(a) Weigh 5 g (to 0.01 g) of the powder after sieving and drying ($M$) in a triangular flask, add 50 mL ($V_1$) of distilled water, shake vigorously for 1 to 2 min, and soak for 24 h. (b) After soaking for 24 h, filter and draw 5 mL ($V_2$) of the filtrate into the triangular flask and add 2 drops of phenolphthalein solution to make the solution appear slightly red. (c) Neutralise with dilute sulphuric acid until colourless. (d) Add 10 drops of potassium chromate indicator. (e) Immediately titrate with $AgNO_3$ solution ($V_3$) to brick red.

See equation (1) when the test is complete.

$$P_1 = \frac{C_{AgNO_3} V_3 \times 0.03545}{GV_2/V_1} \times 100\%, \quad (1)$$

where $P_1$ is the free $Cl^-$ content in the mortar (%); $V_1$ is the volume of silver nitrate solution consumed during each titration (mL); $V_2$ is the volume of filtrate extracted during each titration (mL); $V_3$ is the volume of silver nitrate solution consumed during each titration (mL); $C_{AgNO3}$ is the concentration of $AgNO_3$ (mol/L); and $G$ is the mass of the concrete sample g.

## 3. Test Results and Discussion

*3.1. Compressive and Flexural Strength.* Figure 7 shows the compressive and flexural strengths of two kinds of nanoconcrete. The compressive and flexural strengths of concrete increase significantly after incorporating the nanoparticles, and the compressive and flexural strengths of both nanoconcretes initially increased before decreasing with additional admixture amounts. When higher levels ($A = 3\%$) of two kinds of nanoparticles are mixed, they do not readily disperse and appear agglomerated, which affects the hydration of cement and weakens the compressive and flexural strength of the concrete, so adding more nanoparticles did not improve the strength. The compressive and flexural strengths of concrete clearly improved when $SiO_2$ nanoparticles and $Fe_2O_3$ nanoparticles were mixed at 2% and 1%, respectively. The compressive strength increased by 16.1% and 12.3%, and the flexural strength increased by 15.9% and 12.4%, respectively, compared with ordinary concrete. The improvement of compressive and flexural strengths by nano-$SiO_2$ exceeded that by nano-$Fe_2O_3$.

*3.2. Effect of Nanoparticles on Concrete Durability under the Coupling Effect of Bending Load and Salt Spray Erosion.* Figure 8 shows the relationship between free $Cl^-$, the content of NS and NF, and the nanoparticle admixture (3–5 mm, 7 d, and 30 d was used as an example, and the rest of the depth range has the same law with age); $T$ and C in the figure represent the tensile and compressive zones, respectively; 0, 0.2, 0.3, 0.5, and 0.6 in the figure represent the stress ratio. From Figure 8, the following can be seen:

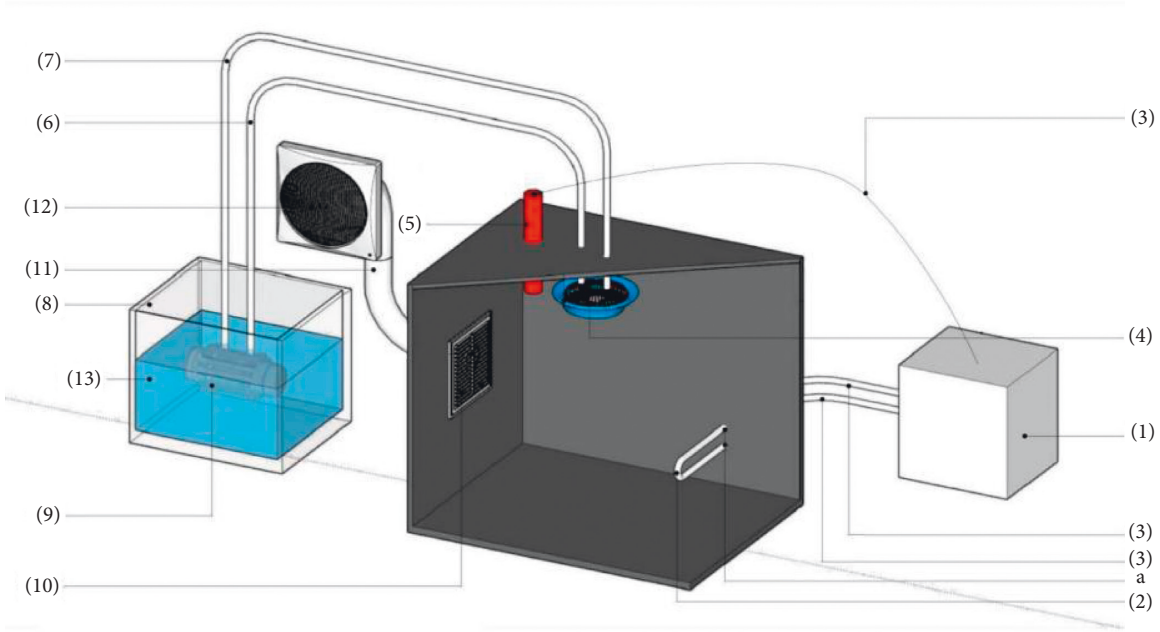


Figure 3: A concrete durability test chamber under salt spray erosion.

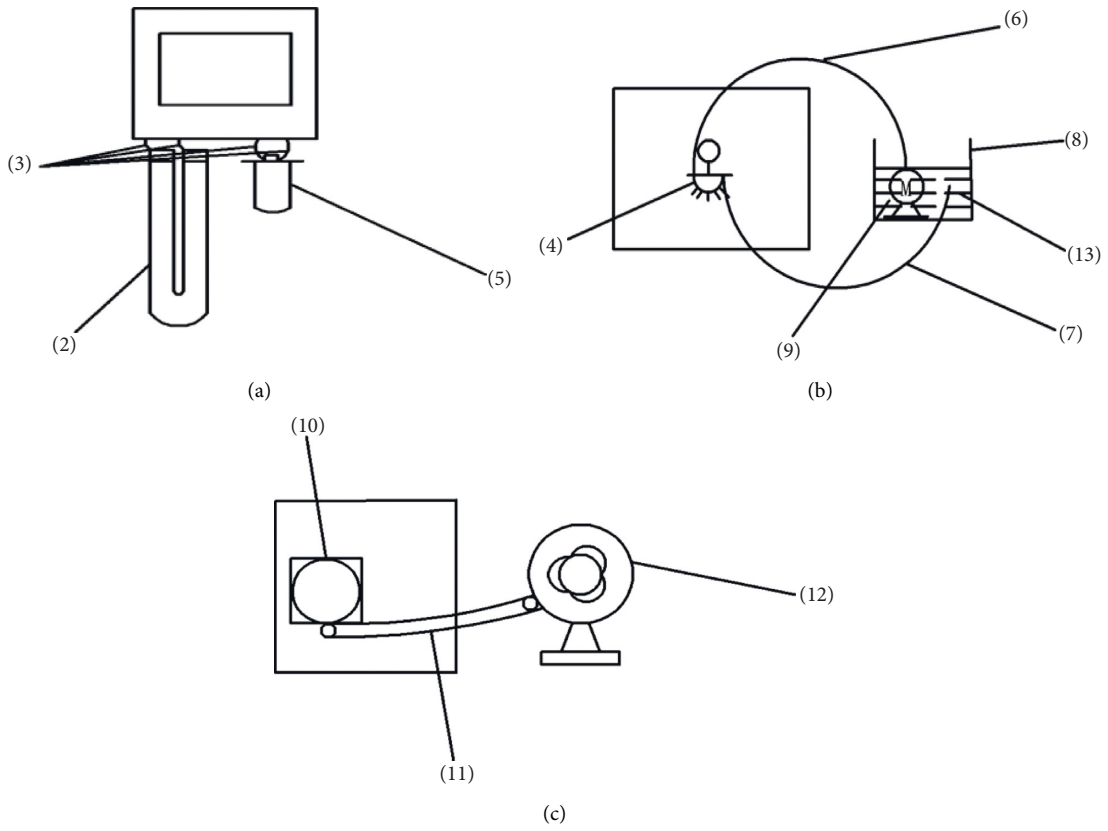


Figure 4: (a) Thermostatic system. (b) Spraying system. (c) Exhaust system.

(1) Free $Cl^-$ in the tensile and compressive zones of nano-$SiO_2$ and nano-$Fe_2O_3$ concrete with different admixtures under different stress conditions are lower than those of ordinary concrete. The above results show that the unique properties of the two nanomaterials, such as the small size effect and the volcanic ash effect, can improve the compactness of the concrete and effectively reduce the $Cl^-$ diffusion


(a) (b) (c)

Figure 5: (a) Drill the powder. (b) Powder samples sorting. (c) 2 h in the oven.

(a) (b) (c) (d) (e)

Figure 6: (a) Distilled water to dissolve samples. (b) Dropoing phenolphthalein. (c) Diluting sulphuric acid neutralized to colourless. (d) Addition of potassium chromate. (e) Titration with $AgNO_3$.

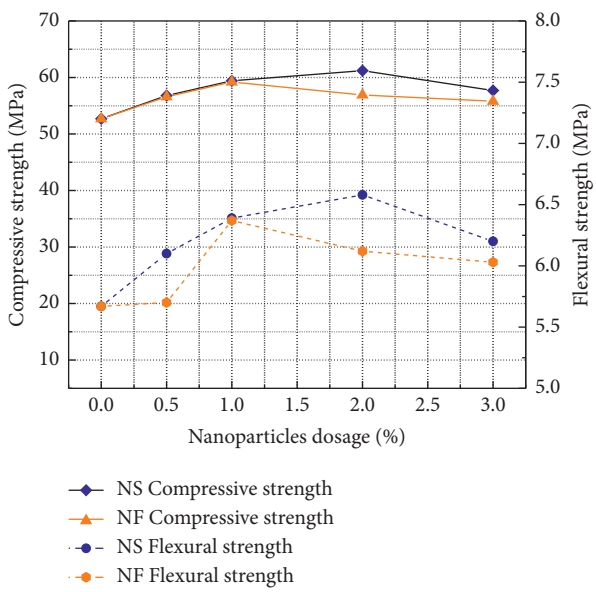


Figure 7: Compressive and flexural strength of nanoconcrete.

rate. So, the admixture of nano-$SiO_2$ and nano-$Fe_2O_3$ finally improved the durability of marine concrete.

(2) Under different stress conditions, the free $Cl^-$ content of both NS and NF initially decreased, then increased with additional admixture, and the free $Cl^-$ contents of nano-$SiO_2$ and nano-$Fe_2O_3$ bottomed out at $A = 2\%$ and $A = 1\%$, respectively. According to the description in Section 3.1, the mechanical properties of the nanomaterials are reduced when they are mixed in excessive amounts due to their prone to agglomeration. This can lead to the internal structure of both nanoconcretes being less dense than when they are mixed at 2% and 1%, respectively, and eventually, the measured free $Cl^-$ content values will match the measured compressive and flexural strengths.

(3) The free $Cl^-$ in the tensile zone of all three concretes (PC, NS, and NF) showed a gradual increase with increasing stress at the same admixture level, and the free $Cl^-$ in the compressive zone gradually decreased with increasing stress. Compared with the unloaded case, when the age at 30 d, the free $Cl^-$ levels in the three concretes increased less when they were

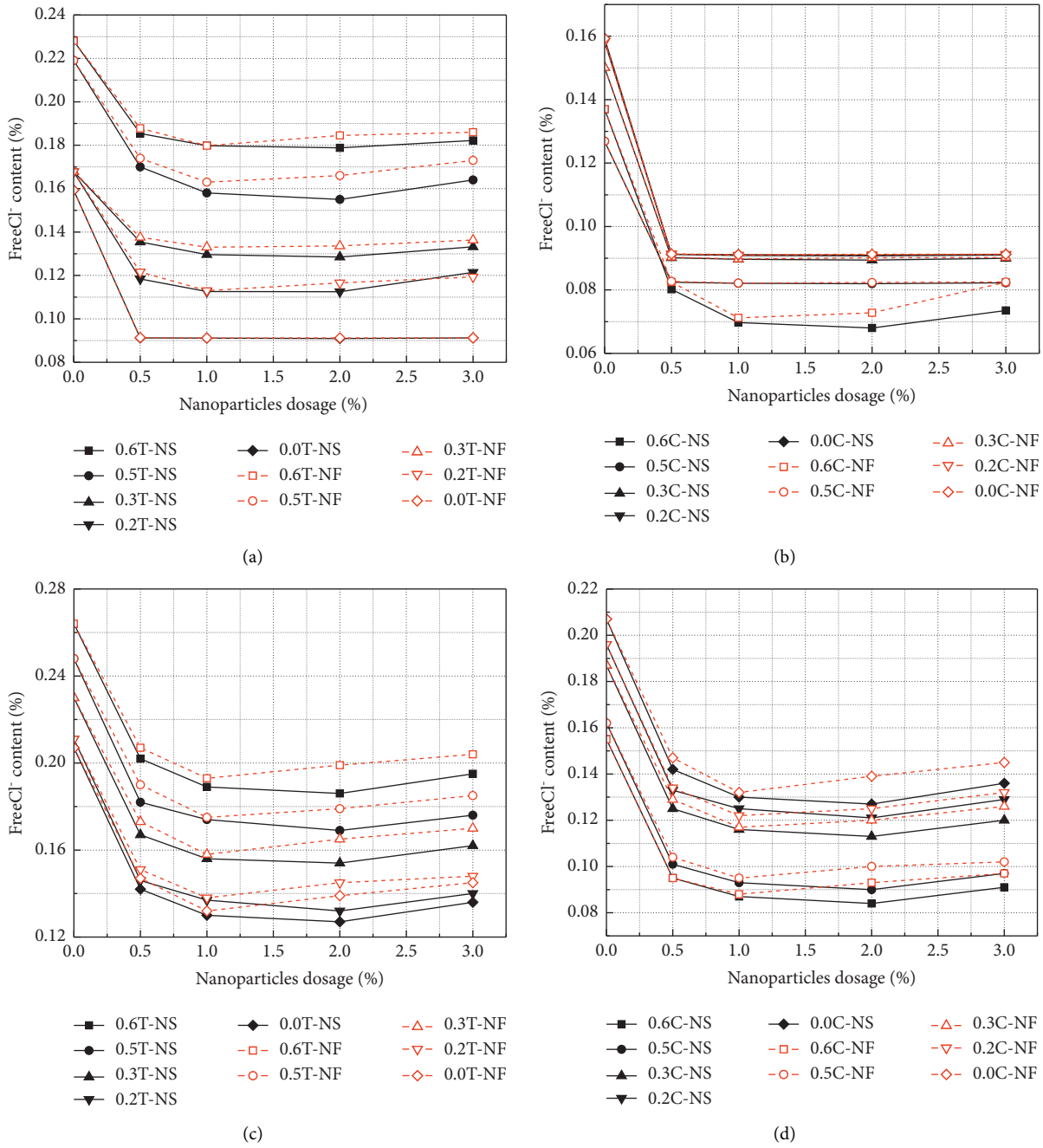


Figure 8: (a) Tensile zone (3–5 mm, 7 d). (b) Compressive zone (3–5 mm, 7 d). (c) Tensile zone (3–5 mm, 30 d). (d) Compressive zone (3-5 mm, 30 d).

subjected to smaller tensile stresses ($\sigma = 0.2$); when $\sigma \geq 0.3$, free $Cl^-$ clearly increased, while free $Cl^-$ in the compressed zone showed a tendency to decrease significantly when the stress was small; however, when the age at 7 d, even the tensile stress is 0.2, the content of free $Cl^-$ increases significantly; in the compressive zone, there was no significant increase in the content of free $Cl^-$. This indicated larger tensile stresses produced more microcracks in the concrete tensile zone with the increase of test age, which deteriorates the $Cl^-$ diffusion resistance of the concrete. The compressive stress increased the compactness of the compressed zone and reduced the $Cl^-$ diffusion path.

(4) The free $Cl^-$ content in NS was basically lower than NF at the same stress and the same admixture, indicating that nano-$SiO_2$ improved the durability performance of nano-marine-concrete under two-factor conditions, which is better than that of nano-$Fe_2O_3$. The above reasons may be due to the volcanic

ash effect of nano-$SiO_2$, which can carry out secondary hydration reactions and consume fragile $Ca(OH)_2$ crystals, making the internal structure of concrete more solid and less susceptible to $Cl^-$ erosion, whereas nano-$Fe_2O_3$ does not have a volcanic ash effect and cannot work with $Ca(OH)_2$ crystals, so the free $Cl^-$ content of NF is higher than that of NS at all dosages.

Figure 9 shows the variation curves of PC, NS20, and NF10-free $Cl^-$ with drilling depth (14 d, $\sigma = 0$,$\sigma = 0.3$, and $\sigma = 0.6$, for example, the other timepoints have the same pattern with stress ratio):

(1) The trend of free $Cl^-$ of loaded and unloaded concrete with depth remained unchanged, and free $Cl^-$ levels decreased with increasing depth, but the free $Cl^-$ content in the tensile zone eclipsed that in the compressive zone at the same depth.

(2) It can be seen from Figures 9(c) and 9(d), the free $Cl^-$ of NS20 and NF10 stabilized at a depth of 10 mm, while PC stabilized beyond 20 mm under the condition of no load. Tensile zone: when $\sigma = 0.3$ and $\sigma = 0.6$, free $Cl^-$ of PC stabilized at 25 mm, while NS20 and NF10 remain stable at the depth range of 20 mm. Compressed zone: the free $Cl^-$ content of PC stabilized at 20 mm, and the free $Cl^-$ levels of NS20 and NF10 were stable at 10 mm.

The above results show that (a) the free $Cl^-$ content of NS20 and NF10 is lower than that of PC at the same depth under both loaded and unloaded conditions, and the depth value at which the free $Cl^-$ content tends to stabilize is also lower than for PC, which again indicates that incorporating nano-$SiO_2$ and nano-$Fe_2O_3$ reduces the salt spray erosion resistance of marine concrete under bending load and the improvement of nano-$SiO_2$ surpassed that of nano-$Fe_2O_3$. (b) Compared with the unstressed condition, the free $Cl^-$ levels in the tensile zones of all three concretes increased, and the free $Cl^-$ in the compressed zone decreased significantly, which again illustrated that the tensile stress action caused more cracks inside the concrete and accelerated $Cl^-$ diffusion. The concrete in the compressed zone would improve with the compressive stress action, which limited further development of microcracks and effectively improved the salt spray erosion resistance of the concrete.

Figure 10 shows the variation curves of free $Cl^-$ content with age for PC, NS20, and NF10 (using a depth of 3–5 mm, $\sigma = 0.2$, and $\sigma = 0.5$ as an example, the rest of the depths have the same pattern with stress ratio).

Figure 10 shows the following: (1) the free $Cl^-$ content of the tensile and compressive zones of the three concretes exhibited the same trend with time, the chloride levels increased with age, and the free $Cl^-$ content of NS20 and NF10 was much lower than PC. (2) Except for the stress ($\sigma = 0.2$) was small, at the same age, free $Cl^-$ in the tensile zone of the three concretes was significantly higher than the compressive zone, which again indicates an increase of microcracks in the tensile zone of the concrete that accelerates $Cl^-$ diffusion. The compressive zone was more well-compacted than the unloaded case due to the compressive stress, which hinders the $Cl^-$ diffusion pathway. The reason for the occurrence of a situation where the free $Cl^-$ content of the concrete in the compression zone will be higher than in the tension zone may be that the stresses applied are small and do not have a significant effect on the structural damage of the concrete. (3) From Figures 9(b) to 9(d), it can be seen that, at the same age, free $Cl^-$ of NF basically exceeded that of NS ($\sigma = 0.5$), which again shows that nano-$SiO_2$ improves the durability performance of marine concrete under the effect of two factors better than nano-$Fe_2O_3$ when the two nanoparticles are in their optimal dosages.

Figure 11 shows the variation of free $Cl^-$ content with stress for PC, NS20, and NF10 (5–10 mm, from 4 d to 30 d is taken as an example, the rest of the depth have the same law).

Figure 11 shows the following: (1) free $Cl^-$ levels for all three types of concrete increased with tensile stress and decreased with the increase of compressive stress. Compared to the unloaded condition (low stress, $\sigma = 0.2$), the free $Cl^-$ content of the tensile and compressive zones increased (decreased) to lesser extents. When $\sigma \geq 0.3$, the free $Cl^-$ increases (decreases) to a greater extent, especially $\sigma = 0.6$, the free $Cl^-$ increases more evidently, which indicated that free $Cl^-$ of the tensile and compressive zones of concrete relates to the stress magnitude. With the gradual increase of tensile stress, the growth rate of internal pores in the tensile zone of the three concrete types accelerates and results in faster diffusion of $Cl^-$ into the concrete interior. The pore structure of the concrete in the compressive zone becomes denser due to the larger compressive stress; this reduced the diffusion rate of $Cl^-$ in the concrete, so with the increase of compressive stress, the concrete better inhibits the effect of $Cl^-$ diffusion.

(2) Under the same stress conditions, in the tensile zone, the free $Cl^-$ content of NS is basically lower than that of NF; this is because the volcanic ash effect of nano-$SiO_2$ promotes the secondary hydration of cement and generates more C-S-H gels; the C-S-H gels increase the denseness of the internal structure of concrete, reduce the generation of unfavorable pores inside the concrete structure, and significantly improve the $Cl^-$ erosion resistance of concrete; while nano-$Fe_2O_3$ does not have the volcanic ash effect and the denseness of its internal structure is not as good as that of NS, so the improvement of NS is better than that of NF.

In the compressive zone, the free $Cl^-$ content of NS is basically the same as that of NF because concrete is a material with good compressive properties, the effect of compressive stress will make its internal structure become denser. The internal structural compactness of the compressive zones in NS and NF achieved the highest when both nanoparticles are at the optimum dosages, which will effectively reduce the $Cl^-$ diffusion pathway, and the measured free $Cl^-$ content depth ranges from 5 to 10 mm, the free $Cl^-$ content in this depth range will be lower, so there will be a small difference between the two types of nano-concrete-free $Cl^-$ content in the compressive zone.

Figure 12 shows the reduction extent of free $Cl^-$ with nanomaterial admixture for NS and NF (using a depth of 3–5 mm 4 d, 21 d, and 30 d as an example):

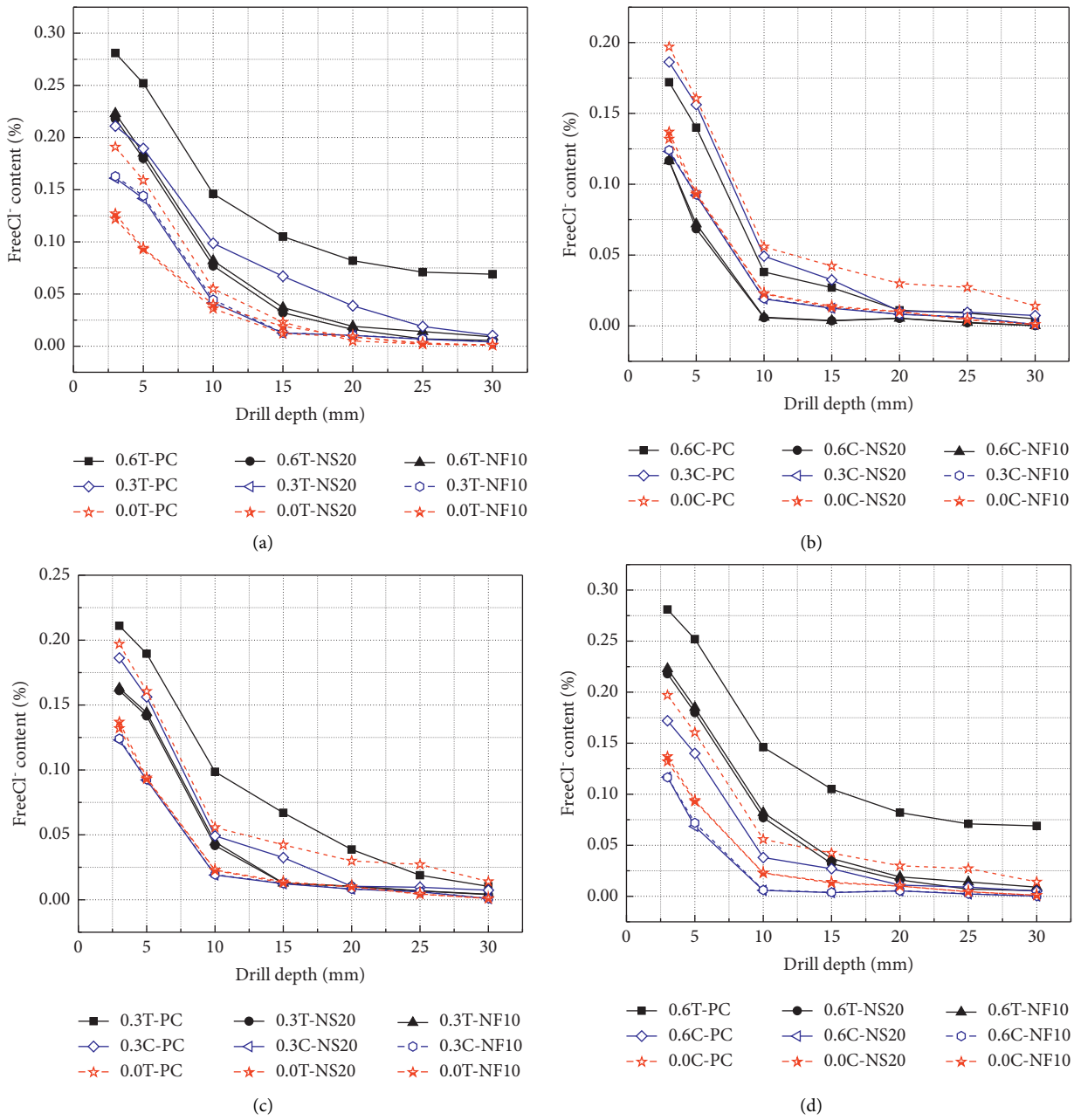


FIGURE 9: (a) Tensile zone. (b) Compressive zone. (c) Comparison between tensile and compressive zones ($\sigma = 0.3$). (d) Comparison between tensile and compressive zones ($\sigma = 0.6$).

(1) Figures 12(a)–12(f) show that, with the increase of admixture, the percentage reduction of free $Cl^-$ for both nanoconcretes under each group of stresses initially increased before decreasing, and the reduction percentage of free $Cl^-$ in the tensile and compressive zones was highest for nano-$SiO_2$ and nano-$Fe_2O_3$ at $A = 2\%$ and $A = 1\%$, respectively.

(2) Figure 12(a) shows the reduction percentages of free $Cl^-$ for NS20 and NF10 were 76.73% and 76.01% when the test age at 4 d under unloaded condition. Figure 12(b) shows that when the test age at 4 d and the stress in the concrete compressive zone is 0.5, the free $Cl^-$ content of NS20 and NF10 decreases by about 1.19 times and 1.13 times, respectively. This indicated that the incorporation of nanoparticles significantly reduced the degree of reinforcement erosion under the coupling of bending load and salt spray erosion.

*3.3. Mechanism for Improving the Durability of Nanoconcrete under the Coupling Effect of Bending Road and Salt Spray Erosion.* Upon exposure to bending load and salt spray erosion, two nanoparticle types improved the durability of marine concrete in primarily two ways: the influence on the

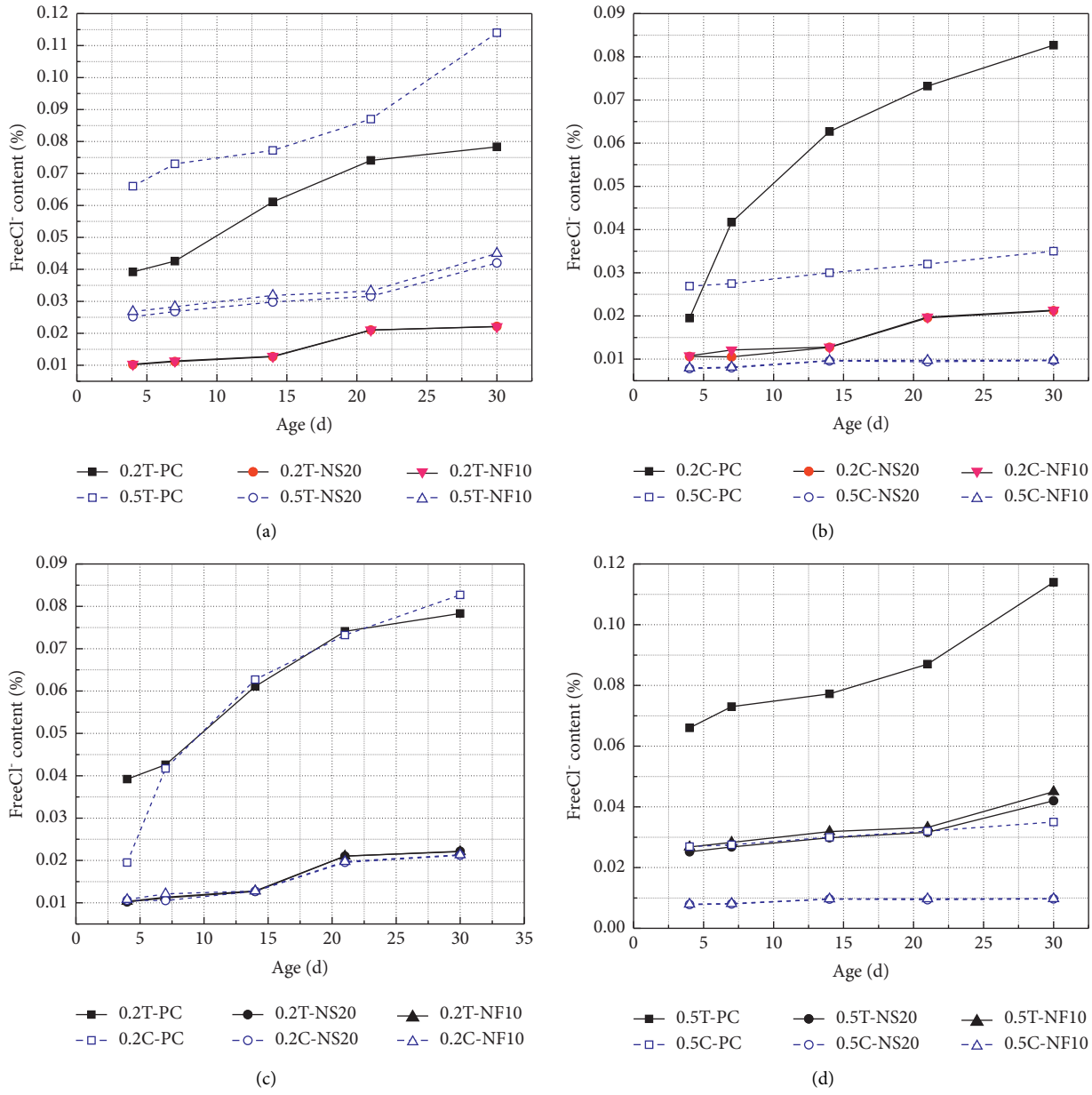


Figure 10: (a) Tensile zone. (b) Compressive zone. (c) Comparison between tensile and compressive zones ($\sigma = 0.2$). (d) Comparison between tensile and compressive zones ($\sigma = 0.5$).

concrete microstructure and the cement hydration product compositions. Both nanoparticles selected have similarities and differences regarding durability improvements. The similarities are reflected in the improvement of the concrete microstructure, and the differences are primarily reflected in the effects on cement hydration.

*3.3.1. Similarities.* The concrete interior primarily contains three types of pores: pores between hydration products, pores between hydrated cement particles, and pores at the interface between cement paste and aggregate. Chloride ions penetrate concrete through these three pores. At larger tensile stresses, the pores of the concrete in the tensile and compressive zones change. Concrete in the tensile zone show increased internal microcracks with increasing tensile stress, adding new pores, which provides an additional $Cl^-$ diffusion "channel." These pores gradually connect to form microcracks; the microcracks become macrocracks, accelerate the rate of $Cl^-$ diffusion in the concrete, reduce the concrete performance against salt spray. Concrete is a material with excellent compressive properties, so the gradually increasing compressive stress compacts the compressed area and inhibits the diffusion rate of $Cl^-$.

Adding nano-$SiO_2$ and nano-$Fe_2O_3$ has a filling effect [22] that effectively fills the concrete pores and reduces the

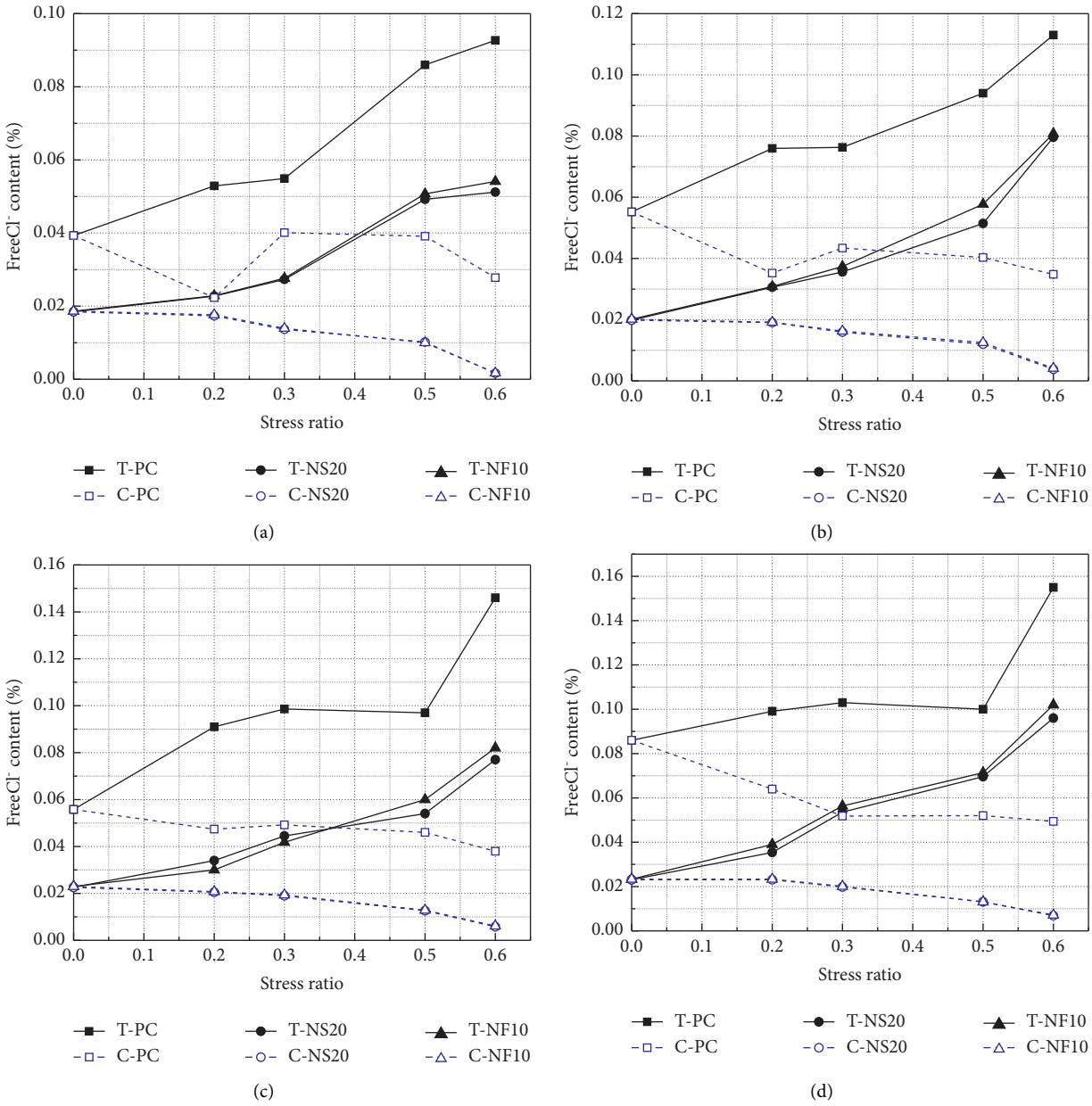


Figure 11: Continued.

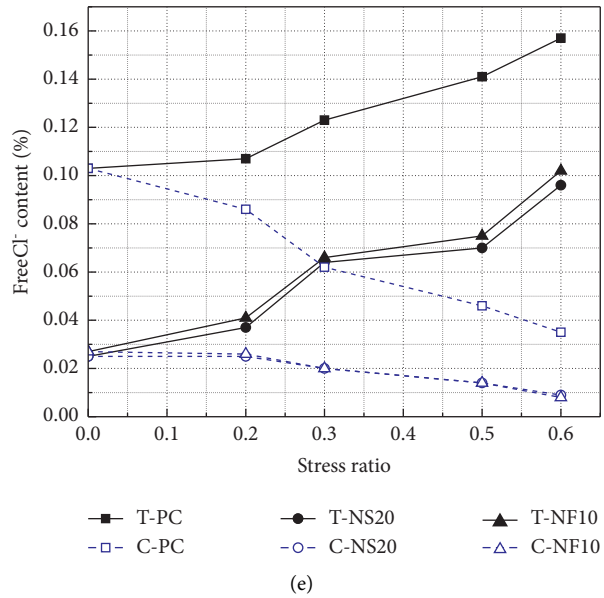


Figure 11: Comparison between tensile and compressive zones: (a) 4 d, (b) 7 d, (c) 14 d, (d) 21 d, and (e) 30 d.

concrete porosity. It also makes the overall concrete structure denser, reduces the generation of cracks, and enhances the durability of marine concrete.

When the concrete sets and hardens, the early cement hydration products include hydrated calcium silicate (C-S-H gel) and $Ca(OH)_2$ crystals. Among them, $Ca(OH)_2$ crystals exist mostly in the interface zone pores between the cement paste and the aggregate [23], which are less stable and lead to the formation of "weak zones" at the interface zone [24]. The "weak zone" is prone to damage when subjected to tensile stress, which deteriorates the pore structure of concrete, increases the diffusion path of $Cl^-$ within the concrete, and reduces the salt spray resistance.

Due to the strong surface effect of nanoparticles, it promotes hydration of cement and increases the number of hydration products (such as C-S-H gel). The "nucleation" effect of nanoparticles [25] causes the hydration products to form a dense skeletal structure around the nanoparticles [26]. This dense skeletal structure inhibits the generation of unfavorable cracks in the tensile zone and reduces the diffusion pathway of $Cl^-$ within the concrete. Therefore, free $Cl^-$ levels in the tensile zone of both NS and NF decrease sharply relative to PC under different stress conditions.

The filling and surface effects of the two nanoparticles incorporated into the concrete eventually improved the internal structure of the concrete and effectively reduced the impact of tensile stress acting on the concrete to produce unfavorable pores and reduced the diffusion channels of $Cl^-$ in the concrete, so that the durability performance of the two nanoconcrete under the action of two factors significantly improved. Tricalcium silicate ($C_3S$) in cement generates $Ca(OH)_2$ crystals and C-S-H gels via hydration. The C-S-H gel distributes irregularly within the concrete (e.g., Figure 11(a)). They nucleate, grow, and gradually aggregate (e.g., Figures 13(b)-13(d)) [27, 28]. A denser C-S-H gel enhances the concrete pore structure and increases the internal compactness of the concrete.

The volcanic ash effect of nano-$SiO_2$ not only accelerates the hydration of $C_3S$ in cement and generates more C-S-H gels [29] but it also promotes secondary hydration of cement (see (1)), consumes unstable $Ca(OH)_2$ crystals, and generates C-S-H gels with lower Ca-Si ratios (Ca/Si). C-S-H gels with lower Ca/Si ratios have better cementing abilities [29] more effectively lower the number of cracks in the concrete due to larger tensile stresses, reduce $Cl^-$ diffusion channels, and improve the salt spray erosion resistance of concrete.

$$x\mathrm{Ca(OH)_2} + \mathrm{SiO_2} + m\mathrm{H_2O} \longrightarrow x\mathrm{CaO \cdot SiO_2 \cdot} m\mathrm{H_2O} \quad (2)$$

Tricalcium aluminate ($C_3A$) reacts with gypsum ($CaSO_4{\cdot}2H_2O$) in cement when it meets water to form an aft phase ($3CaOAl_2O_3{\cdot}3CaSO_4{\cdot}32H_2O$) (see equations (3) and (4)). The hydration product aft phase is shaped like needles and rods, which can form a dense spatial skeleton with C-S-H gels and aggregates [30].Chloride ions that replace $SO_4^{2-}$ in the aft phase can form Friedel's salt [31], which improves $Cl^-$ binding capacity. Chloride ions also react with $C_3A$ to form Friedel's salt ($C_3A{\cdot}CaCl_2{\cdot}10H_2O$) (equation (5)) [32].

$$3\mathrm{CaO \cdot Al_2O_3} + 12\mathrm{H_2O} + \mathrm{Ca(OH)_2} \longrightarrow 4\mathrm{CaO \cdot Al_2O_3 \cdot 13H_2O} \quad (3)$$

$$4\mathrm{CaO \cdot Al_2O_3 \cdot 13H_2O} + 3\left(\mathrm{CaSO_4 \cdot 2H_2O}\right) + 14\mathrm{H_2O} \longrightarrow 3\mathrm{CaO \cdot Al_2O_3 \cdot 3CaSO_4 \cdot 32H_2O} + \mathrm{Ca(OH)_2} \quad (4)$$

$$\mathrm{C_3A} + 2\mathrm{NaCl} + \mathrm{Ca(OH)_2} + 10\mathrm{H_2O} \longrightarrow \mathrm{C_3A \cdot CaCl_2 \cdot 10H_2O} + 2\mathrm{Na^+} + 2\mathrm{OH^-} \quad (5)$$

Friedel's salts fill the concrete pores and reduce their porosity [33].The incorporation of nano-$SiO_2$, which has a volcanic ash effect, accelerates hydration and increases levels

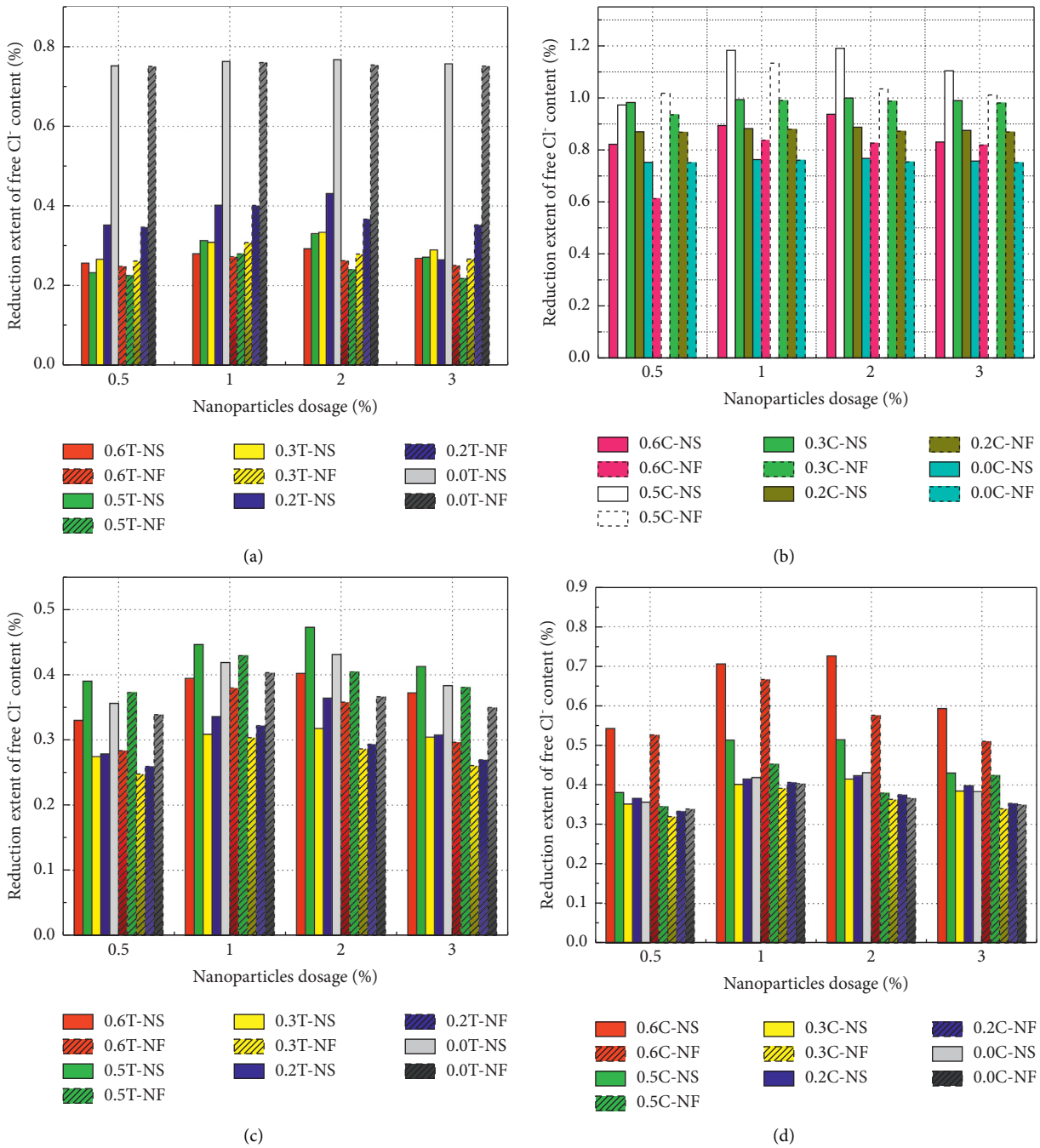


Figure 12: Continued.

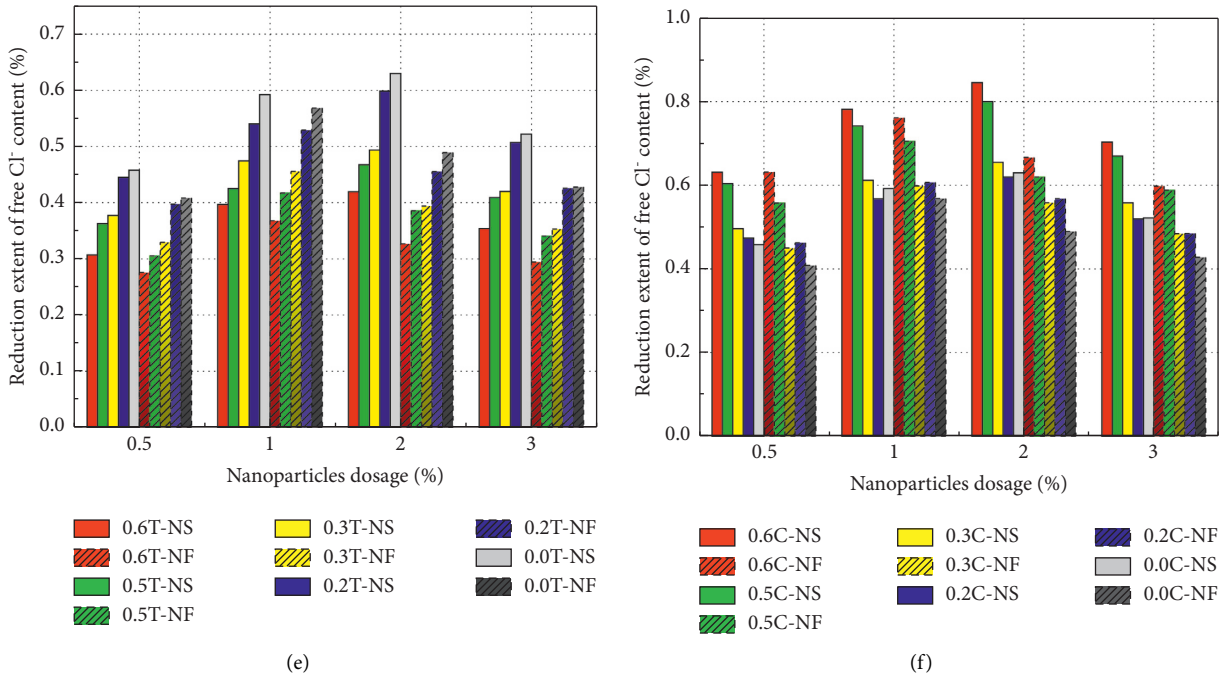


Figure 12: (a) Tensile zone (4 d). (b) Compressive zone (4 d). (c) Tensile zone (21 d). (d) Compressive zone (21 d). (e) Tensile zone (30 d). (f) Compressive zone (30 d).

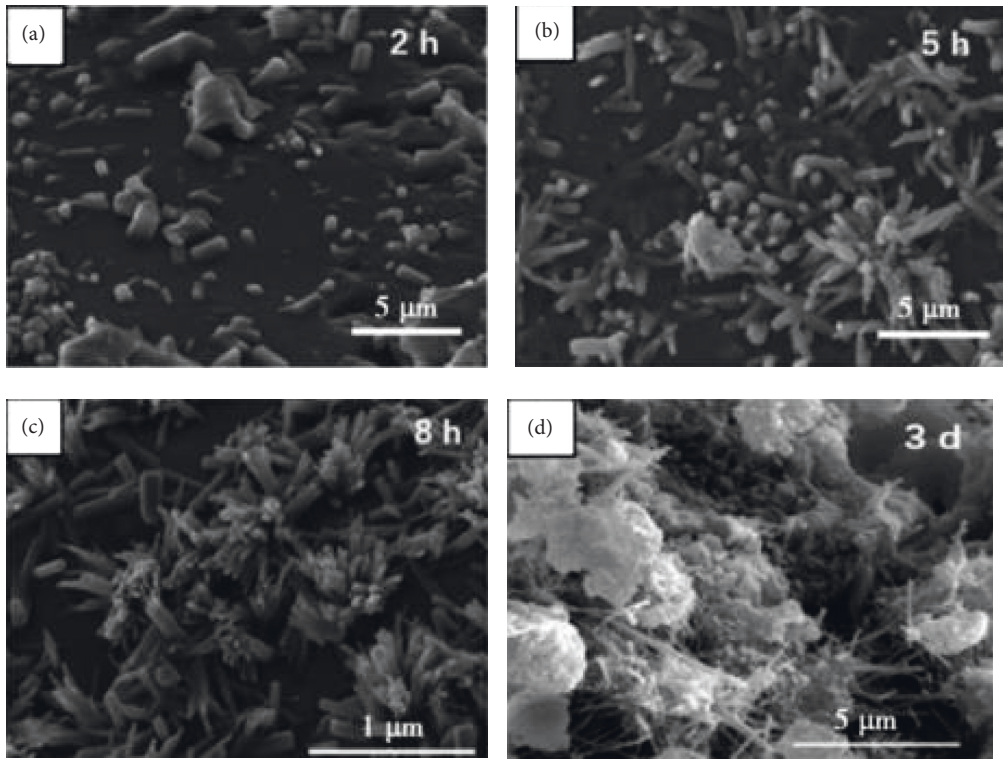


Figure 13: Variation of C-S-H morphology with hydration time [27, 28].

of Friedel's salt that ultimately leads to increased durability of the offshore concrete structure when subjected to the marine environment.

Nano-$Fe_2O_3$ has no volcanic ash effect and does not react with $Ca(OH)_2$ [34]. However, nano-$Fe_2O_3$ can adsorb $Ca^{2+}$ in the concrete pore solution [35] to form numerous lumpy

products containing principally two elements, Ca and O, which densely aggregate have no apparent cracks on the surface, [36]and do not have "unstable" $Ca(OH)_2$ crystals. The newly formed dense bulk products reduce the amount of $Ca^{2+}$ in the pore solution, resulting in the production of fewer $Ca(OH)_2$ crystals. This thick lumpy product readily improves the negative effect of the internal "weak zone" of NF and reduces the impact of microcracks on concrete due to tensile stress, which agrees with the above test result that free $Cl^-$ levels in NF with different admixtures dramatically drop relative to PC at the same stress and age. Levels of free $Cl^-$ in NF were also dramatically lower relative to PC at the same stress and age, which also agreed with the above test results.

In summary, the volcanic ash activity of nano-$SiO_2$ and the adsorption property of nano-$Fe_2O_3$ improved the overall structural compactness of concrete, reduced the diffusion path of $Cl^-$ and the influence of cracks in weak areas, and improved the durability of marine concrete under the effects of bending load and salt spray erosion.

## 4. Conclusions

(1) The 28 d compressive strength and flexural strength of both nanoconcretes were higher than PC, the compressive strength increased by 16.1% and 12.3%, and the flexural strength increased by 15.9% and 12.4% for nano-$SiO_2$ and nano-$Fe_2O_3$, respectively, at optimized dosing ($A = 2\%$ and $A = 1\%$, respectively).

(2) Incorporating nano-$SiO_2$ and nano-$Fe_2O_3$ lowered levels of free $Cl^-$ for each admixture related to ordinary concrete, which improved salt spray erosion resistance of concrete subjected to flexural loading. The improvement of nano-$SiO_2$ surpassed those of nano-$Fe_2O_3$. At the same depth and timepoint, free $Cl^-$ levels for both nanoconcretes decreased when tensile stress increases and increased with additional compressive stress.

(3) The free $Cl^-$ amounts for both nanoparticles decreased with increasing depths. At the same depths, free $Cl^-$ levels for both NS20 and NF10 in the tensile and compressive zones were significantly lower than PC. Free $Cl^-$ in both NS20 and NF10 increased with time, and the free $Cl^-$ content in the tensile zone was basically much higher than the compressive zone. When the test age at 4 d, the reduction percentages of free $Cl^-$ for NS20 and NF10 were 76.73% and 76.01% under unloaded condition, and the stress in concrete compressive zone is 0.5, the free $Cl^-$ content of NS20 and NF10 decreases by about 1.19 times and 1.13 times, respectively.

(4) The filling and surface effects of nano-$SiO_2$ and nano-$Fe_2O_3$ effectively improved the internal structure of concrete and resulted in lower porosity and denser structures. This hindered the development of internal microcracks in the concrete structure and inhibited transport of $Cl^-$ inside the concrete, which ultimately improved the durability of marine concrete.

(5) The volcanic ash effect of nano-$SiO_2$ promoted the generation of an aft phase and Friedel's salt. The aft phase not only improved the overall compactness of the concrete structure but also generated Friedel's salt by replacing $SO_4^{2-}$ with $Cl^-$. Nano-$Fe_2O_3$ adsorbed $Ca^{2+}$ into the concrete pore solution and formed many dense block hydration products, reduced the weak areas of concrete, and finally improved the durability performance of marine concrete upon exposure to a marine environment.

(6) In marine engineering, the marine concrete in salt spray areas can be based on the ratio of ordinary concrete and replace cement with nano-$SiO_2$ ($A = 2\%$) or nano-$Fe_2O_3$ ($A = 1\%$) in equal amounts to achieve significant improvements in the durability of marine concrete under simultaneous exposure to bending loads and salt spray erosion.

According to the research content of this work, two more points can be further investigated to better meet the durability performance design of marine engineering as follows:

(a) This paper focuses on the study of the durability of nano-marine-concrete under the action of bending load and salt spray erosion; in actual marine engineering, many buildings are also subjected to fatigue loads, and the durability of nano-marine-concrete under the coupling effect of fatigue load and salt spray erosion can be further studied.

(b) The effect of free $Cl^-$ content on the erosion damage of nanoconcretes under bending load has been investigated in this work, and the effects of bound $Cl^-$ content and total $Cl^-$ content on nano-concrete under external load can be investigated next.

## Data Availability

Data are available on reasonable request from the corresponding author.

## Disclosure

The patent number used in this article (ZL202120853835.7), and the patent name is "a concrete durability test chamber under salt spray erosion."

## Conflicts of Interest

The authors declare no conflicts of interest.

## Authors' Contributions

Zhang Maohua conceptualized the study, provided resources, reviewed and edited the manuscript, supervised the study, was responsible for project administration, and acquired funding. Lv Zhengyi contributed to methodology, investigated the study, and prepared the original draft. Lv Zhengyi and Cui Jiyin validated the study; Lv Zhengyi, Cui

Jiyin, Tian Zenong, and Li Zhiyi were responsible for formal analysis.

## Acknowledgments

This work was supported by the National Natural Science Foundation of China (52078109).

## References

[1] Li Su, D. Niu, D. Huang, Y. Luo, H. Qiao, and Y. Zhang, "Chloride diffusion behavior and microstructure of basalt-polypropylene hybrid fiber reinforced concrete in salt spray environment," *Construction and Building Materials*, vol. 324, Article ID 126716, 2022.

[2] D. Huang, D. Niu, and Li Su, "Diffusion of chloride ion in coral aggregate seawater concrete under marine environment [J]," *Construction and Building Materials*, vol. 284, Article ID 122821, 2021.

[3] Q. Liu, Z. Hu, X.-er Wang et al., "Numerical study on cracking and its effect on chloride transport in concrete subjected to external load," *Construction and Building Materials*, vol. 325, no. 28, Article ID 126797, 2022.

[4] J. Mao, F. Xu, Wl Jin, J. Zhang, Xx Wu, and Cs Chen, "Research on the fatigue flexural performance of RC beams attacked by salt spray," *China Ocean Engineering*, vol. 32, no. 2, pp. 179–188, 2018.

[5] J. Xu, T. Zhao, J. Wu, and B. Diao, "Experimental study and reliability assessment of fatigue loaded reinforced concrete beams combined with chloride exposure," *Construction and Building Materials*, vol. 322, no. 7, Article ID 126480, 2022.

[6] Y. Lu, W. Tang, S. Li, and M. Tang, "Effects of simultaneous fatigue loading and corrosion on the behavior of reinforced beams," *Construction and Building Materials*, vol. 181, pp. 85–93, 2018.

[7] J. Wu, J. Xu, B. Diao, and D. K. Panesar, "Impacts of reinforcement ratio and fatigue load level on the chloride ingress and service life estimating of fatigue loaded reinforced concrete (RC) beams," *Construction and Building Materials*, vol. 266, no. 7, Article ID 120999, 2021.

[8] J. Wu, B. Diao, J. Xu, R. Zhang, and W. Zhang, "Effects of the reinforcement ratio and chloride corrosion on the fatigue behavior of RC beams," *International Journal of Fatigue*, vol. 131, Article ID 105299, 2020.

[9] Q. Fu, M. Bu, Z. Zhang et al., "Chloride ion transport performance of lining concrete under coupling the action of flowing groundwater and loading," *Cement and Concrete Composites*, vol. 123, Article ID 104166, 2021.

[10] H. S. Shang, J. H. Zhou, G. X. Fan, Gt Yang, and Wj You, "Study on the bond behavior of steel bars embedded in concrete under the coupling of sustained loads and chloride ion erosion," *Construction and Building Materials*, vol. 276, no. S2, Article ID 121684, 2021.

[11] B. Qi, J. Gao, F. Chen, and D. Shen, "Chloride penetration into recycled aggregate concrete subjected to wetting-drying cycles and flexural loading," *Construction and Building Materials*, vol. 174, pp. 130–137, 2018.

[12] S. Li, S. Yin, L. Wang, and X. Hu, "Mechanical properties of eccentrically compressed columns strengthened with textile-reinforced concrete under the coupled action of chloride salt corrosion and loading," *Applied Ocean Research*, vol. 116, Article ID 102884, 2021.

[13] Q. Zhou, C. Lu, W. Wang, S. Wei, C. Lu, and M. Hao, "Effect of fly ash and sustained uniaxial compressive loading on chloride diffusion in concrete," *Journal of Building Engineering*, vol. 31, Article ID 101394, 2020.

[14] T. Cao, L. Zhang, G. Sun et al., "Simulation of chloride ion transport in concrete under wetting–drying cycle," *Construction and Building Materials*, vol. 241, Article ID 118045, 2020.

[15] J. Wang, P. M. Basheer, S. V. Nanukuttan, A. E. Long, and Y. Bai, "Influence of service loading and the resulting micro-cracks on chloride resistance of concrete," *Construction and Building Materials*, vol. 108, pp. 56–66, 2016.

[16] Z. Meng, Q.-feng Liu, W. She, Y. Cai, J. Yang, and M. Farjad Iqbal, "Electrochemical deposition method for load-induced crack repair of reinforced concrete structures: a numerical study," *Engineering Structures*, vol. 246, Article ID 112903, 2021.

[17] T. Horiguchi and N. Saeki, *Assessment of Chloride Penetration into Fiber Reinforced concrete under Loading*, pp. 717–724, Thomas Telford Publishing, London, UK, 2005.

[18] D. Huang, D. Niu, H. Zheng, L. Su, D. Luo, and Q Fu, "Study on chloride transport performance of eco-friendly coral aggregate concrete in marine environment," *Construction and Building Materials*, vol. 258, Article ID 120272, 2020.

[19] M. Zhang and Y. Sun, "$Cl^-$ penetration resistance of nano-particles under the action of dry-wet cycle," *Journal of Harbin Institute of Technology*, vol. 51, no. 8, p. 10, 2019 (in Chinese).

[20] Y. Gao, W. Zhou, W. Zeng, G. Pei, and K Duan, "Preparation and flexural fatigue resistance of self-compacting road concrete incorporating nano-silica particles," *Construction and Building Materials*, vol. 278, no. S1, Article ID 122380, 2021.

[21] Ru Mu and An Yan, "Damage and damage suppression of HPC under freeze-thaw and stress composite effects," *Journal of Building Materials*, no. 04, pp. 359–364, 1999, (in Chinese).

[22] H. Li, M. Zhang, and J. Ou, "Abrasion resistance of concrete containing nano-particles for pavement," *Wear*, vol. 260, no. 11-12, pp. 1262–1266, 2006.

[23] B. Liang, *Mechanical Properties Test and Microstructure Analysis of Nano-$SiO_2$ Ultrafine Fly Ash concrete*, Master's thesis, Anhui University of Science& Technology, Huainan, 2018, in Chinese.

[24] T. Kefeng, "Research on the performance of light aggregate and high-performance light aggregate concrete," *Journal of Tongji University*, vol. 34, no. 4, pp. 472–475, 2006, (in Chinese).

[25] S. Wu, S. Dai, and B. Ma, "Effect of nano-$SiO_2$ on steel slag cement-based cementitious materials," *Silicate Bulletin*, vol. 40, no. 5, pp. 1594–1600, 2021, (in Chinese).

[26] B. W. JoJo, C. H. Kim, Gh Tae, and J. B. Park, "Characteristics of cement mortar with nano-SiO2 particles," *Construction and Building Materials*, vol. 21, no. 6, pp. 1351–1355, 2007.

[27] E. Berodier and K. Scrivener, "Understanding the filler effect on the nucleation and growth of C-S-H," *Journal of the American Ceramic Society*, vol. 97, no. 12, pp. 3764–3773, 2014.

[28] X. Liu, P. Feng, and X. Shen, "Research progress on hydrated calcium silicate (C-S-H), a hydration product of cement," *Materials Report*, vol. 35, no. 09, pp. 9157–9167, 2021, (in Chinese).

[29] W. J. Wang, *Research on Curing Mechanism and Damage Characteristics of Nano-mineral Powder Hydroclay*, Ph.D.thesis, Zhejiang University, Hangzhou, 2004, in Chinese.

[30] S. Xu, "Study on the Effect and mechanism of nano-$SiO_2$ endogenous generation on cementitious materials," Master's

Thesis, China University of Mining and Technology, Beijing, 2019, in Chinese.

[31] F. Xing, J. Liu, B. Dong, and Y. Huo, "Combination procedure and mechanism of sea sand type chlorine ions with cement materials," *Journal of Southeast University (Natural Science Edition)*, vol. 36, pp. 167–172, 2006.

[32] P. K. Mehta, "Effect of cement composition on erosion of reinforcing steel in concrete," *Chloride Erosion of Steel in Concrete Cement and Concrete Research*, vol. 21, no. 5, pp. 777–794, 1991.

[33] R. Hooton, A. Suryavanshi, and R. Swamy, "Influence of penetrating chlorides on the pore structure of structural concrete," *Cement, Concrete and Aggregates*, vol. 20, no. 1, p. 169, 1998.

[34] H. Xiao, *Study on the Preparation Process and Multifunctional Characteristics of Smart concrete with Superfine Particles*, Master's thesis, Harbin Institute of Technology, Harbin, 2002, in Chinese.

[35] X. Lu, L. Huang, and L. Yang, "Research progress on the preparation method of iron oxide nano-particles nano-particles," *Applied Chemistry*, vol. 46, no. 4, pp. 741–743, 2017, (in Chinese).

[36] Z. Yunzhe, *Research on the Salt-Freezing Resistance of Nano-Modified concrete and its Modification Mechanism*, Master's thesis, Harbin Institute of Technology, Harbin, 2015, in Chinese.